

# Ring Currents in a Proposed System Containing Planar Hexacoordinate Carbon, $\text{CB}_6^{2-}$

Remco W. A. Havenith, Patrick W. Fowler,\* and Erich Steiner<sup>[a]</sup>

**Abstract:** Current-density maps at the coupled Hartree–Fock level calculated in the CTOCD (continuous transformation of origin of current density) approach demonstrate the magnetic response of the hypothetical planar hexacoordinate carbon species,  $\text{CB}_6^{2-}$ . In contrast with the empty  $\text{B}_6^{2-}$  framework,

which supports paramagnetic currents, the carbon-containing species has a typical diamagnetic  $\pi$ -ring current that

**Keywords:** aromaticity • electronic structure • hexacoordinate carbon • ring currents

circulates undisturbed by the central atom. In spite of the unconventional nature of the species, the properties of  $6\pi \text{CB}_6^{2-}$  and  $4\pi \text{B}_6^{2-}$  can be rationalised with the same orbital model that accounts for the diamagnetic  $\pi$  current of benzene and the paramagnetic  $\pi$  current of planar cyclooctatetraene.

## Introduction

The edifice of systematic organic stereochemistry has as its cornerstone the tetrahedral disposition of the four valences of saturated carbon.<sup>[1, 2]</sup> Nevertheless, even this near-universal rule has its exceptions. Predicted planar geometries for carbon in fourfold coordination<sup>[3–7]</sup> have been verified in a small number of cases,<sup>[8–11]</sup> and in recent theoretical explorations of the boundaries of carbon chemistry,<sup>[12, 13]</sup> even more exotic planar *hexacoordinate* carbon atoms have been proposed for species such as  $\text{CB}_6^{2-}$ . One motivation given by Exner and Schleyer for considering such high coordination numbers was the potential for discovery of new aromatic systems.<sup>[12]</sup> One popular probe of aromaticity on the magnetic criterion is the NICS (nucleus-independent chemical shift)<sup>[14]</sup> computed at or above ring centres and compared with a benzene standard. Such comparisons are less clearcut for systems with a central atom, but the computed shifts at 1.0 and 1.5 Å above the ring centre ( $\delta = -22.8 / -9.7$ ) have been taken to suggest aromaticity<sup>[12]</sup> for  $\text{CB}_6^{2-}$ . Herein we take up this theme and explore the consequences of the unusual hexacoordinate bonding environment directly for the main diagnostic of aromaticity: the ring current<sup>[14–17]</sup> itself.

Ring currents can be visualised directly from *ab initio* theory using coupled Hartree–Fock theory in the CTOCD (continuous transformation of origin of current density) approach for the calculation of the induced current densi-

ty.<sup>[18, 19]</sup> Advantages of this approach are practical, in that it gives well converged results with modest basis sets,<sup>[20, 21]</sup> and conceptual, in that it provides an analysis in terms of readily interpretable orbital contributions that are, in a well-defined sense, optimal.<sup>[22]</sup> The CTOCD method is applied here to the predicted<sup>[12]</sup>  $\text{CB}_6^{2-}$  species.

## Computational Methods

The geometries of  $\text{CB}_6^{2-}$  ( $D_{6h}$  symmetry) and  $\text{B}_6^{2-}$  ( $D_{2h}$  symmetry) were calculated at the RHF/6-311 + G\* level of theory, using GAMESS-UK.<sup>[23]</sup> Hessian calculations at the optimised geometries show that both lie at true local minima of the potential energy hypersurfaces at this level of theory. The magnetic properties of  $\text{CB}_6^{2-}$  and  $\text{B}_6^{2-}$  were computed by using distributed-origin methods, at the coupled Hartree–Fock level, with the SYSMO program,<sup>[24]</sup> using the 6-311 + G\* basis set. Current-density maps were plotted by using the DZ (diamagnetic zero) variant of the CTOCD method, where the current density at any point in space is calculated with that point as origin.<sup>[25]</sup> This *ipsocentric* choice of gauge is crucial to the calculation of orbital contributions that are uncontaminated by occupied–occupied mixing.<sup>[22]</sup> Current densities induced by a unit magnetic field acting along the principal axis were plotted in a plane  $1a_0$  above that of the ring (that is, close to the maximum  $\pi$  density, where the current is essentially parallel to the molecular plane), in a plotting area of  $16 \times 16 a_0^2$ . In Figures 1–4, contours denote the modulus of the current density at values  $0.001 \times 4^n eh/2\pi m_e a_0^4$  for  $n=0, 1, 2, \dots$ , and vectors represent in-plane projections of current. In all plots, diamagnetic circulation is shown anti-clockwise and paramagnetic circulation clockwise.

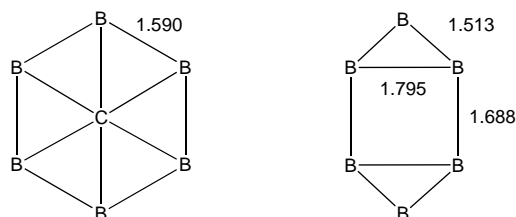
## Results

### The $\text{CB}_6^{2-}$ dianion

**Geometry:** In agreement with the calculations of Exner and Schleyer,<sup>[12]</sup> this system is found to have a minimum with  $D_{6h}$  symmetry, and the bond lengths of 1.590 Å are compatible

[a] Prof. P. W. Fowler, Dr. R. W. A. Havenith, Dr. E. Steiner  
School of Chemistry, University of Exeter  
Stocker Road, Exeter, EX4 4QD (UK)  
Fax: (+44) 1392-263434  
E-mail: P.W.Fowler@exeter.ac.uk

with those calculated at the density functional theory (DFT) level (Scheme 1; B3LYP/6-311 + G\*: 1.594 Å).<sup>[12]</sup> As the hexagon is regular, the B–B and B–C distances are of course equal. The lowest vibrational frequency is 315 cm<sup>-1</sup> (cf.



Scheme 1. RHF/6-311 + G\* geometries of  $\text{CB}_6^{2-}$  and  $\text{B}_6^{2-}$  (bond lengths in Å).

270 cm<sup>-1</sup> in the DFT calculation of reference [12]) and this indicates local stability against rearrangement for this species, at least at sufficiently low temperatures. The electronic configuration is [(core)<sup>14</sup>(3a<sub>1g</sub>)<sup>2</sup>(2e<sub>1u</sub>)<sup>4</sup>(2e<sub>2g</sub>)<sup>4</sup>(1a<sub>2u</sub>)<sup>2</sup>(4a<sub>1g</sub>)<sup>2</sup>(2b<sub>1u</sub>)<sup>2</sup>-(3e<sub>1u</sub>)<sup>4</sup>(1e<sub>1g</sub>)<sup>4</sup>].

As a doubly charged anion, the system has a positive HOMO eigenvalue in this finite basis, indicative of its instability to autoionisation, unless embedded in a protecting lattice or solvation shell.

**Ring currents:** Figure 1 shows maps of a)  $\sigma$ , b)  $\pi$  and c) total ( $\sigma + \pi$ ) induced current densities, all plotted in the 1a<sub>0</sub> plane. The  $\sigma$ -only map (Figure 1 a) shows a set of local paramagnetic vortices over the boron sites, and a central diamagnetic flow around the carbon site at the ring centre. This pattern is an interesting reversal of the normal  $\sigma$  map for hydrocarbon rings,<sup>[26]</sup> where localised diamagnetic bond circulations build up a *paramagnetic* circulation at the ring centre. There is little indication of localised B–B or B–C bond circulations in Figure 1 a, and the atom at the hexagon centre acts as a centre of circulation in its own right.

The  $\pi$ -only map (Figure 1 b) exhibits a typical diamagnetic ring current, characteristic of aromatic species such as benzene, and apparently uninfluenced by the presence of the central atom. This independence of the carbon atom from the  $\pi$  system of the boron framework is consistent with its lack of a suitable low-lying d orbital—it cannot participate without such an orbital in the 1e<sub>1g</sub>  $\pi$  HOMO of the framework, which as we will see later, is the dominant contributor to the ring current.

Superposition of  $\sigma$  and  $\pi$  current densities in the total map (Figure 1 c) gives a reinforced diamagnetic circulation both inside and outside the ring, with small paramagnetic eddies over the boron sites, similar to those observed in other maps of B-containing species.<sup>[27]</sup>

The current densities in  $\text{CB}_6^{2-}$  (or  $\text{C@B}_6^{2-}$  as it might be called in endohedral cluster notation) can be further analysed to reveal specific orbital characteristics. In the CTOCD-DZ formulation, the induced current density at each point in space can be written as a sum over virtual transitions from each occupied orbital to the whole manifold of unoccupied orbitals.<sup>[22]</sup> The sum is dominated by low-energy transitions, that is in the best case between orbitals near the HOMO–

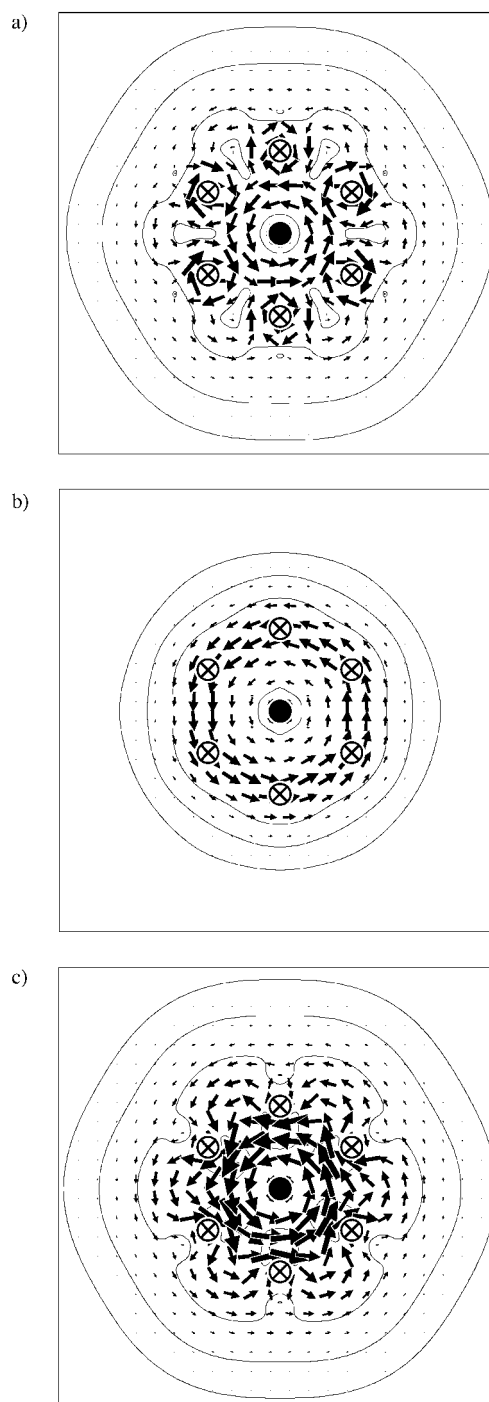


Figure 1. Maps of current density in  $\text{CB}_6^{2-}$ : a)  $\sigma$ -only, b)  $\pi$ -only and c) ( $\sigma + \pi$ ) current (● carbon, ⊗ boron; nuclear positions projected to the plotting plane).

LUMO frontier, and is governed by symmetry-based selection rules. “Diamagnetic” contributions are those allowed under in-plane translational excitation of occupied orbitals and “paramagnetic” contributions are those allowed under in-plane rotational excitation of occupied orbitals. This means that for  $\text{CB}_6^{2-}$ , in  $D_{6h}$  symmetry, the product symmetry  $\Gamma(\psi_n) \times \Gamma(\psi_p)$  for a transition from the occupied orbital  $\psi_n$  to the virtual orbital  $\psi_p$  must contain  $A_{2g}$  for rotationally allowed and  $E_{1u}$  for translationally allowed transitions. In most systems

examined so far, the total induced  $\pi$ -current density is dominated by just a few electrons.<sup>[28]</sup>

The orbital-by-orbital analysis of the current density of  $\text{CB}_6^{2-}$  (shown in Figure 2) reveals that the global current  $1a_0$  above the molecular plane is dominated by the contributions of three sets of occupied molecular orbitals. These are the

pair ( $\varepsilon = -0.172 E_h$ ) complete the localised paramagnetic eddies on the boron sites.

**Discussion:** A rationalisation of individual orbital contributions can be given in terms of qualitative cluster-bonding theory, which allows identification of the available excitations

into the lowest-lying unoccupied molecular orbitals. A particular transition from an occupied to an unoccupied molecular orbital will have a large current-density if the target orbital is the translational or rotational partner of the occupied orbital, and if the energy gap is sufficiently small.<sup>[22]</sup> The dominant transitions between occupied molecular orbitals and their partners are depicted in Scheme 2. Occupied orbitals are shown on the left, their partners on the right. The descriptions of symmetries and transition types that apply to  $\text{CB}_6^{2-}$  are indicated in red.

Starting at the top of the scheme, each member of the  $1e_{1g}$  HOMO pair of  $\text{CB}_6^{2-}$  can be connected to either of the two  $\pi^* 1e_{2u}$  orbitals by multiplication with  $x$  or  $y$ , introducing an extra nodal plane in one or two ways. Thus symmetry, nodal matching and energy gap factors all conspire to produce a significant orbital current density (Figure 2a), in agreement with the dominant rôle of the HOMO in the  $\pi$  ring current (Figure 1b). In a pure Hückel model of benzene, this HOMO–LUMO transition would give the sole contribution to the  $\pi$  current.<sup>[28]</sup>

The next pair of orbitals in Scheme 2 are the ( $\sigma$ ) radial cluster-bonding  $3e_{1u}$  set, which again are each converted to an antibonding partner by multiplication with either  $x$  or  $y$  and so give an overall diamagnetic contribution (Figure 2b).

The next orbital in Scheme 2 is the non-degenerate  $1b_{1u}$  tangential cluster-bonding orbital, which can be converted by a concerted rotation on each boron site into the fully antibonding radial combination, and hence, obeys the requirements for a paramagnetic contribution (Figure 2c). This transition would be blocked in conventional aromatics and antiaromatics by the filling of the target orbital as part of the set of C–H bonds.

Finally, the  $2e_{2g}$  pair exhibits a set of tangential-to-radial transitions on concerted rotation, and hence gives a para-

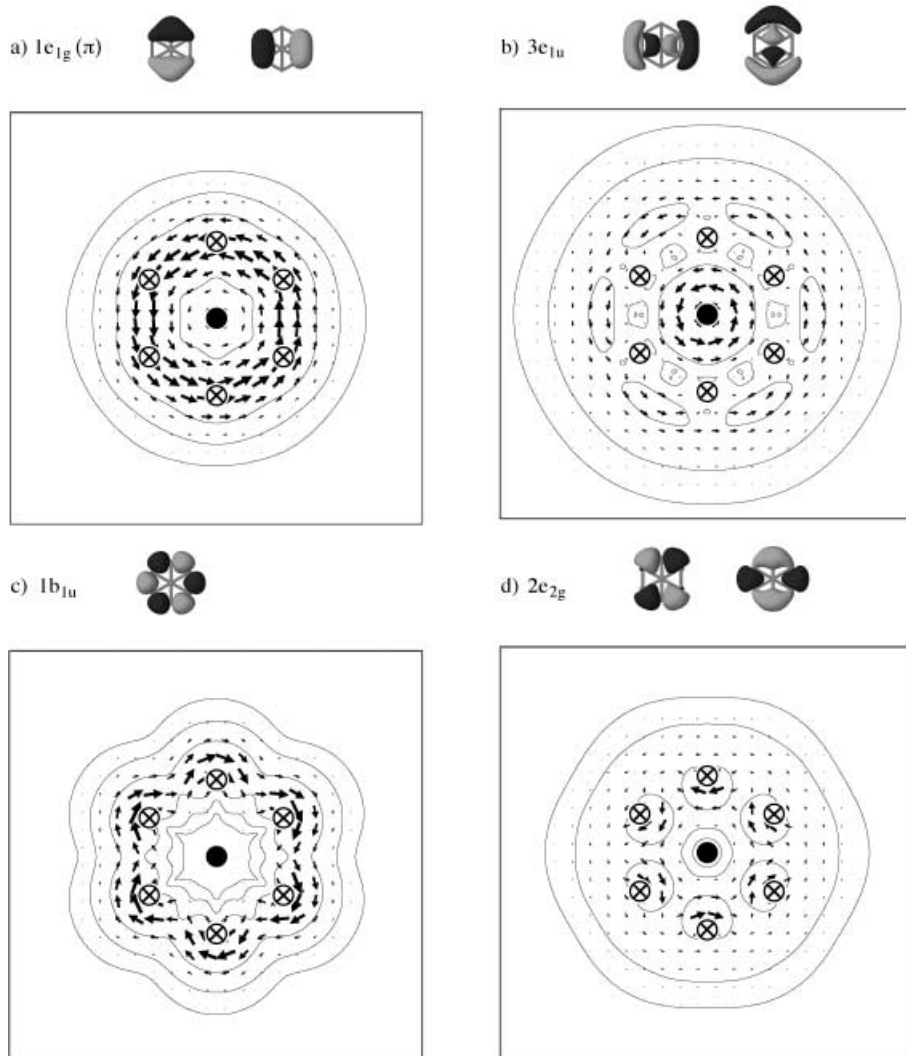
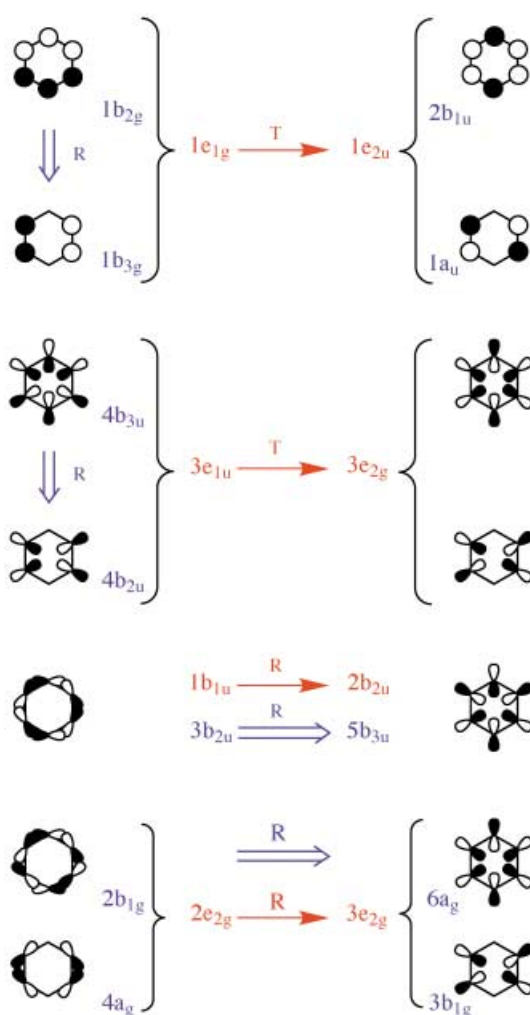


Figure 2. Contour plots for the most magnetically active  $\text{CB}_6^{2-}$  molecular orbitals, showing their contributions to the total current density.

degenerate  $\pi$  HOMO ( $1e_{1g}$ , RHF/6-311+G\* orbital energy  $\varepsilon = 0.102 E_h$ ), which contributes essentially the whole of the diatropic  $\pi$ -ring current (cf. Figure 2a and 1b), the HOMO-1 carbon–boron  $\sigma$ -bonding combinations ( $3e_{1u}$ ,  $\varepsilon = -0.034 E_h$ ), which contribute most of the diamagnetic current over the centre of the molecule, and the HOMO-2 tangential boron–boron bonding orbital ( $1b_{1u}$ ,  $\varepsilon = -0.071 E_h$ ), which gives the main paramagnetic contribution to the circulation on the outside of the molecule. Neither of the next two orbitals in the energy sequence,  $4a_{1g}$  ( $\varepsilon = -0.145 E_h$ , a bonding combination of carbon  $2s$  and in-plane radial boron  $2p$  orbitals), and  $1a_{2u}$  ( $\varepsilon = -0.162 E_h$ , the bonding combination of carbon  $2p_z$  and in-phase  $2p_\pi$  orbitals on boron), contribute any significant current density. Small contributions from the HOMO-5  $2e_{2g}$



Scheme 2. Schematic representation of the dominant transitions in  $\text{CB}_6^{2-}$  (red) and  $\text{B}_6^{2-}$  (blue). T denotes translationally allowed transitions (yielding diamagnetic currents) and R denotes rotationally allowed transitions (yielding paramagnetic currents).

magnetic contribution (Figure 2d), which in  $\text{CB}_6^{2-}$  is less significant than the contribution of  $1b_{1u}$ , as would be expected from the larger energy denominator. Again, these target orbitals would be unavailable in conventional unsaturated hydrocarbon systems.

### A comparison with the $\text{B}_6^{2-}$ dianion

**Geometry:** A wealth of minima with different geometries and spin multiplicities exists on the potential energy surface of neutral  $\text{B}_6$ .<sup>[29–31]</sup> Minima with different spin multiplicities can also be located on the potential energy surface of the dianion  $\text{B}_6^{2-}$ , but for our purpose of comparing the ring currents and molecular orbitals of  $\text{B}_6^{2-}$  with those of  $\text{CB}_6^{2-}$  we have limited our search to minima with planar geometries. Calculations constrained to  $D_{6h}$  symmetry gave no minimum. However, a singlet, closed-shell configuration was located for  $\text{B}_6^{2-}$  in  $D_{2h}$  symmetry at the RHF/6-311 + G\* level of theory. Its geometry is shown in Scheme 1.

At this local minimum (lowest vibrational frequency  $274\text{ cm}^{-1}$ )  $\text{B}_6^{2-}$  has 16 doubly occupied molecular orbitals,

corresponding to the configuration  $[(\text{core})^{12}(3a_g)^2(3b_{3u})^2(2b_{2u})^2(4a_g)^2(2b_{1g})^2(1b_{1u})^2(3b_{2u})^2(5a_g)^2(4b_{3u})^2(1b_{2g})^2]$ .

The correlation rules for descent from  $D_{6h}$  to  $D_{2h}$  are:  $A_1 \rightarrow A$ ,  $A_2 \rightarrow B_1$ ,  $B_1 \rightarrow B_2$ ,  $B_2 \rightarrow B_3$ ,  $E_1 \rightarrow B_2 + B_3$ ,  $E_2 \rightarrow A + B_1$  and  $g \rightarrow g$ ,  $u \rightarrow u$ . The  $1b_{2g}$  HOMO and  $4b_{3u}$  HOMO-1 of  $\text{B}_6^{2-}$  are the low-energy members of the split  $1e_{1g}$  HOMO and  $3e_{1u}$  HOMO-1 pairs of  $\text{CB}_6^{2-}$ , each of which also give rise to an unoccupied orbital of  $\text{B}_6^{2-}$ . As a consequence, the empty framework of  $\text{B}_6^{2-}$  has four  $\pi$  electrons, in contrast with the six  $\pi$  electrons of the carbon-filled  $\text{CB}_6^{2-}$ .

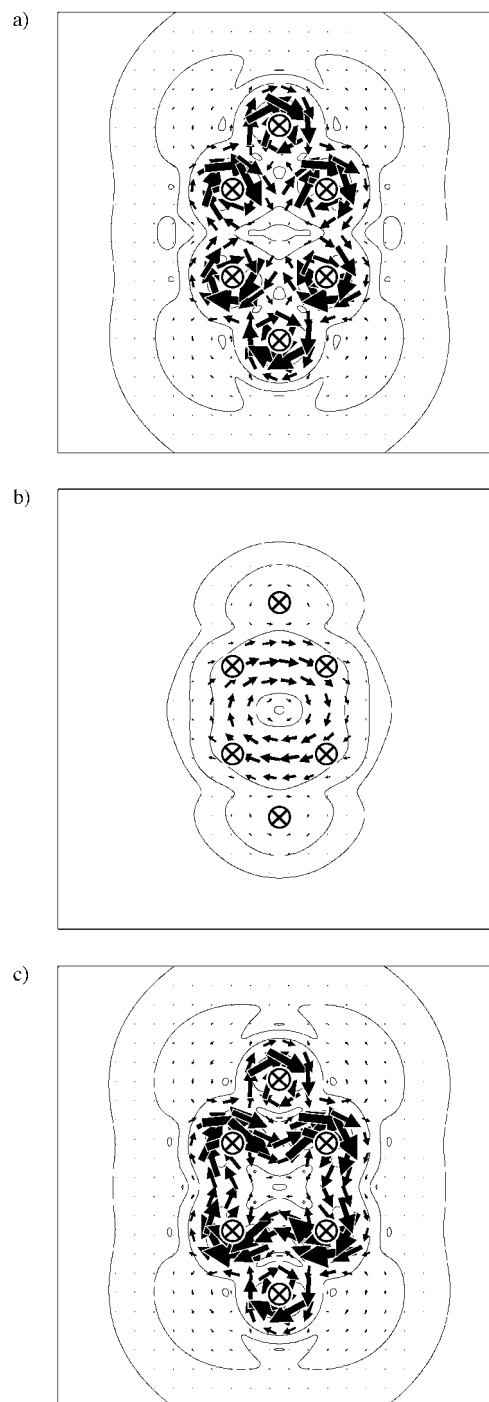


Figure 3. Maps of current density in  $\text{B}_6^{2-}$  ( $D_{2h}$  symmetry): a)  $\sigma$ -only, b)  $\pi$ -only and c)  $(\sigma + \pi)$  current ( $\otimes$  boron; nuclear positions projected to the plotting plane).

**Ring currents:** Figure 3 shows the calculated a)  $\sigma$ -only, b)  $\pi$ -only and c) total ( $\sigma + \pi$ ) current-density maps for the  $D_{2h}$ -symmetric  $B_6^{2-}$  ion. The  $\sigma$  map (Figure 3a) shows, as for  $CB_6^{2-}$ , local paramagnetic circulations around the boron atoms, but unlike the  $CB_6^{2-}$  map has no clear single central diamagnetic component. In both the  $\pi$ -only and ( $\sigma + \pi$ ) maps, a strong paramagnetic current is discernible in the inner square of the molecule, consistent with the expected  $4\pi$ -electron anti-aromatic nature of this system. A NICS value of  $\delta = 2.21$ , computed at the ring centre in the present basis, using the CTOCD-PZ2<sup>[25]</sup> method is consistent with a paratropic current. The ( $\sigma + \pi$ ) map shows also local paramagnetic circulations around the two boron atoms located outside the central square.

**Discussion:** The orbital-by-orbital analysis of the currents in  $B_6^{2-}$ , shown in Figure 4, allows the marked differences from the maps for  $CB_6^{2-}$  to be rationalised in terms of the electron configuration. The blue labels and arrows in Scheme 2 refer to  $B_6^{2-}$ . In  $D_{2h}$  symmetry, the orbital product symmetries for rotationally allowed transitions contain  $B_{1g}$ , and for translationally allowed transitions contain  $B_{2u}$  or  $B_{3u}$ . The total

current density in  $B_6^{2-}$  is dominated by four non-degenerate orbitals. The contribution of the four dominant molecular orbitals, namely  $2b_{1g}$ ,  $3b_{2u}$ ,  $4b_{3u}$  and  $1b_{2g}$ , is in all cases paramagnetic.

The splitting of the degenerate  $1e_{1g}$   $\pi$  pair, into one filled ( $1b_{2g}$ ; HOMO;  $\epsilon = 0.072 E_h$ ) and one empty ( $1b_{3g}$ ;  $\epsilon = 0.313 E_h$ ) orbital has a dramatic effect on the induced current density contribution of the  $\pi$  electrons. There is now a rotationally allowed transition within the split pair (indicated by the vertical blue arrow in Scheme 2), and the sense of the current therefore changes from diamagnetic to paramagnetic. A similar rotational transition between a symmetry-split  $\pi$  pair is responsible for the paratropicity of the  $4n$  annulenes.<sup>[28]</sup>

In the manifold of radial-cluster orbitals, a similar new rotationally allowed transition appears between the  $(4b_{3u})^2$  (HOMO-1;  $\epsilon = 0.057 E_h$ ) and  $(4b_{2u})^0$  ( $\epsilon = 0.271 E_h$ ) components of the original  $(3e_{1u})^4$  pair, resulting in the destruction of the central diamagnetic current of  $CB_6^{2-}$ .

The current-density contributions of the  $2b_{1g}$  and  $3b_{2u}$  orbitals of  $B_6^{2-}$  are similar to those of the parent  $2e_{2g}$  and  $1b_{1u}$  orbitals of  $CB_6^{2-}$ : in both species there are allowed concerted rotational transitions (see Scheme 2).

As a consequence of the rise in energy of  $(2b_{1g})^2$  and fall of the target  $(6a_g)^0$  induced by the symmetry-splittings  $2e_{2g} \rightarrow 2b_{1g} + 4a_g$  and  $3e_{2g} \rightarrow 6a_g + 3b_{1g}$ , the paramagnetic current in  $B_6^{2-}$  attributable to these two electrons is stronger than the rather weak contribution from the four electrons of  $(2e_{2g})^4$  in  $CB_6^{2-}$ .

## Conclusion

A modern distributed-gauge method has been used to identify the magnetic response of a species containing carbon in a novel hexacoordinate environment. Insertion of a carbon atom into the  $B_6^{2-}$  ring has a decisive effect on the properties. Whereas the empty boron ring supports a paratropic  $\pi$  current,  $CB_6^{2-}$  supports an apparently normal diatropic  $\pi$  current, which circulates undisturbed around the encapsulated carbon atom, as carbon lacks the low-lying d orbital necessary for participation in the framework orbitals that dominate the current.

A breakdown of the total current into physically distinct orbital contributions can be

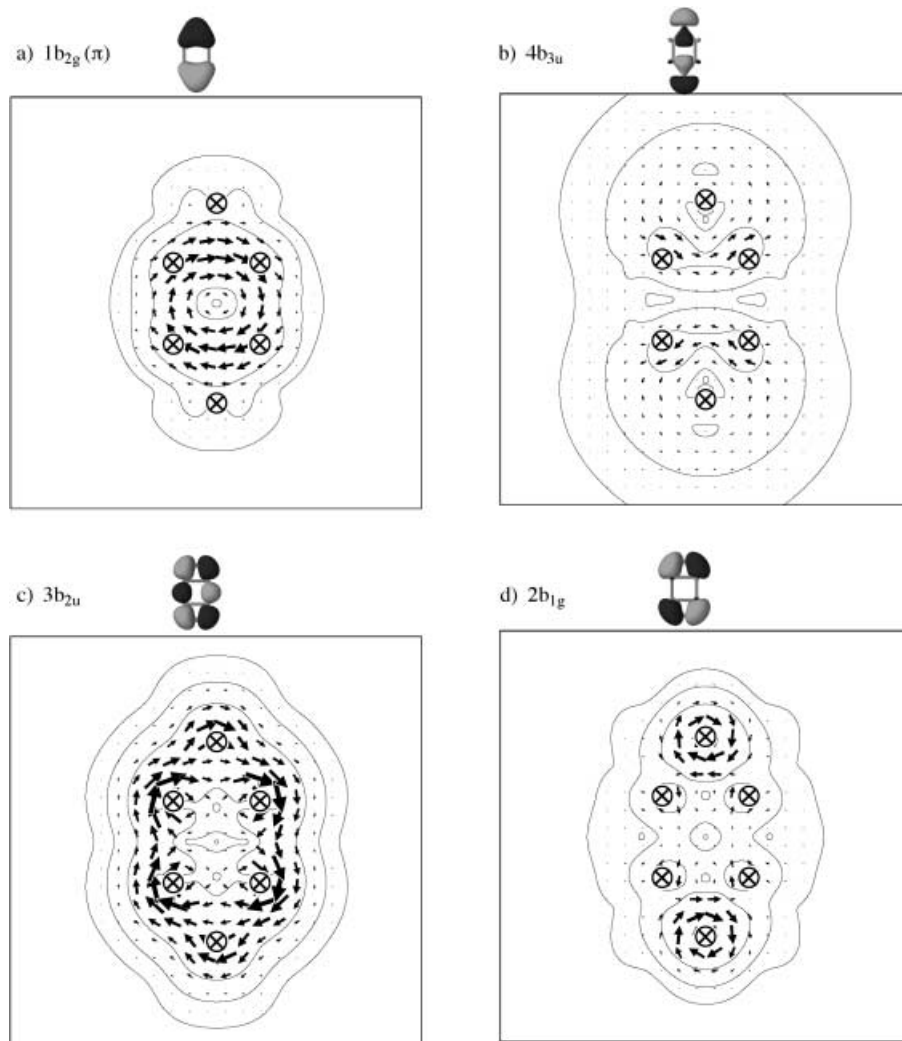


Figure 4. Contour plots for the most magnetically active  $B_6^{2-}$  molecular orbitals, showing their contributions to the total current density.

made, taking advantage of the ipsocentric CTOCD-DZ formalism. In contrast with conventional carbon-based aromatics, the coordinative unsaturation of the boron atoms leads to low-lying  $\sigma$  orbitals and, hence, a significant paratropic contribution to the  $\sigma$  ring current on the perimeters of both  $\text{CB}_6^{2-}$  and  $\text{B}_6^{2-}$ . In spite of their unconventional nature,  $\text{CB}_6^{2-}$  and  $\text{B}_6^{2-}$  have the  $\pi$  currents expected of  $6\pi$  and  $4\pi$  planar monocycles. In  $\text{CB}_6^{2-}$  the diatropic current is attributable to the four HOMO electrons, as in benzene. In  $\text{B}_6^{2-}$  the two HOMO electrons occupy half of a symmetry-split pair connected by a rotationally allowed transition and hence give rise to a paramagnetic  $\pi$  current, as in the planar form of the antiaromatic cyclooctatetraene.

### Acknowledgement

We thank the European Union TMR scheme, contracts FMRX-CT097-0192 and FMRX-CT096-0126, for partial financial support.

- [1] J. A. le Bel, *Bull. Soc. Chim. Fr. II* **1874**, 22, 337.  
 [2] J. H. van't Hoff, *Bull. Soc. Chim. Fr. II* **1875**, 23, 295.  
 [3] R. Hoffmann, R. W. Alder, C. F. Wilcox, Jr., *J. Am. Chem. Soc.* **1970**, 92, 4992.  
 [4] J. B. Collins, J. D. Dill, E. D. Jemmis, Y. Apeloig, P. von R. Schleyer, R. Seeger, J. A. Pople, *J. Am. Chem. Soc.* **1976**, 98, 5419.  
 [5] P. von R. Schleyer, A. I. Boldyrev, *J. Chem. Soc. Chem. Commun.* **1991**, 1536.  
 [6] D. Rasmussen, L. Radom, *Angew. Chem.* **1999**, 111, 3052; *Angew. Chem. Int. Ed.* **1999**, 38, 2876.  
 [7] Z.-X. Wang, P. von R. Schleyer, *J. Am. Chem. Soc.* **2001**, 123, 994.  
 [8] S. Harder, J. Boersma, L. Brandsma, A. van Heteren, J. A. Kanters, W. Bauer, P. von R. Schleyer, *J. Am. Chem. Soc.* **1988**, 110, 7802.  
 [9] F. A. Cotton, M. Shang, *J. Am. Chem. Soc.* **1990**, 112, 1584.  
 [10] G. Erker, R. Zwitter, *J. Am. Chem. Soc.* **1990**, 112, 9620.  
 [11] D. Röttger, G. Erker, *Angew. Chem.* **1997**, 109, 840; *Angew. Chem. Int. Ed. Engl.* **1997**, 36, 812.  
 [12] K. Exner, P. von R. Schleyer, *Science* **2000**, 290, 1937.  
 [13] Z.-X. Wang, P. von R. Schleyer, *Science* **2001**, 292, 2465.  
 [14] P. von R. Schleyer, C. Maerker, A. Dransfeld, H. Jiao, N. J. R. van Eikema Hommes, *J. Am. Chem. Soc.* **1996**, 118, 6317.  
 [15] L. Pauling, *J. Chem. Phys.* **1936**, 4, 673.  
 [16] F. London, *J. Phys. Radium* **1937**, 8, 397.  
 [17] J. A. Pople, *J. Chem. Phys.* **1956**, 24, 1111.  
 [18] T. A. Keith, R. F. W. Bader, *Chem. Phys. Lett.* **1993**, 210, 223.  
 [19] S. Coriani, P. Lazzeretti, M. Malagoli, R. Zanasi, *Theoret. Chim. Acta* **1994**, 89, 181.  
 [20] T. A. Keith, R. F. W. Bader, *J. Chem. Phys.* **1993**, 99, 3669.  
 [21] R. Zanasi, P. Lazzeretti, M. Malagoli, F. Piccinini, *J. Chem. Phys.* **1995**, 102, 7150.  
 [22] E. Steiner, P. W. Fowler, *J. Phys. Chem. A* **2001**, 105, 9553.  
 [23] M. F. Guest, J. H. van Lenthe, J. Kendrick, K. Schöffel, P. Sherwood, R. J. Harrison, GAMESS-UK, a package of ab initio programs, **2000**. With contributions from R. D. Amos, R. J. Buenker, H. J. J. van Dam, M. Dupuis, N. C. Handy, I. H. Hillier, P. J. Knowles, V. Bonačić-Koutecký, W. von Niessen, R. J. Harrison, A. P. Rendell, V. R. Saunders, A. J. Stone, D. J. Tozer and A. H. de Vries. It is derived from the original GAMESS code due to M. Dupuis, D. Spangler, J. Wendolowski, *NRCC Software Catalog, Vol. I*, Program No. QG01 (GAMESS) **1980**.  
 [24] P. Lazzeretti, R. Zanasi, SYSMO package (University of Modena), **1980**. Additional routines for evaluation and plotting of current density, E. Steiner, P. W. Fowler.  
 [25] R. Zanasi, *J. Chem. Phys.* **1996**, 105, 1460.  
 [26] E. Steiner, P. W. Fowler, *Int. J. Quantum Chem.* **1996**, 60, 609.  
 [27] I. Černušák, P. W. Fowler, E. Steiner, *Mol. Phys.* **2000**, 98, 945.  
 [28] E. Steiner, P. W. Fowler, *Chem. Commun.* **2001**, 2220.  
 [29] A. K. Ray, I. A. Howard, K. M. Kanal, *Phys. Rev. B* **1992**, 45, 14247.  
 [30] I. Boustani, *Phys. Rev. B* **1997**, 55, 16426.  
 [31] J. Niu, K. Rao, P. Jena, *J. Chem. Phys.* **1997**, 107, 132.

Received: September 3, 2001 [F3525]